Reactivity of Surface Lewis and Brønsted Acid Sites in Zeolite Catalysis – A Computational Case Study of DME Synthesis Using H-SSZ-13

Philipp Huber,[†] Felix Studt[†,‡] and Philipp N. Plessow[*,†]

[†]Institute of Catalysis Research and Technology, Karlsruhe Institute of Technology, Hermann-von-Helmholtz Platz 1, 76344 Eggenstein-Leopoldshafen, Germany

[‡]Institute for Chemical Technology and Polymer Chemistry, Karlsruhe Institute of Technology, Engesserstrasse 18, 76131 Karlsruhe, Germany

Supporting Information Placeholder

ABSTRACT: The stability and reactivity of Lewis and Brønsted acid sites at the H-SSZ-13 surface are investigated for the (101) and (001) surfaces. We focus on the conversion of methanol to dimethyl ether (DME) as a probe reaction that is prototypical for the reactivity of acidic zeolites, for example in the methanol-to-olefins process. We use periodic density functional theory (DFT) calculations in combination with highly accurate DLPNO-CCSD(T) calculations on cluster models. At Brønsted acid sites, DME can be formed via the concerted and the stepwise mechanism. The barriers for acid sites located at the surface are comparable to those located in the bulk. DME formation on a Lewis acid site is similar to the concerted mechanism, since two adsorbed methanol molecules react with each other directly. However, the oxygen of the adsorbed methanol is bound to the Al atom and an analogy can therefore also be drawn with a methoxy group and thus the second step of the stepwise mechanism on Brønsted acid sites. The barriers for DME formation on a Lewis acid site are more similar to the concerted mechanism of the Brønsted acid sites and are therefore at 400°C significantly higher than the stepwise mechanism at Brønsted acid sites.

KEYWORDS: zeolites, Brønsted acidity, Lewis acidity, H-SSZ-13, DFT, ab-initio, methanol, DME

INTRODUCTION:

Acidic zeolites are important in many chemical processes and are expected to play a key role for a sustainable economy relying on renewable resources.[1] One application is the direct conversion of biomass, for example through the dehydration of alcohols.[2] Another promising area is the conversion of methanol obtained from biomass via syngas. In the methanol-to-olefins (MTO) and methanol-to-gasoline processes, hydrocarbons with desired functionality can be obtained by utilizing suitable catalysts and through proper control of reaction conditions.[3-4] The reaction networks of the MTO process determining the selectivity and reactivity are complex and heavily intertwined.[5-6] This is hence one area of zeolite catalysis where quantum chemical calculations, typically based on density functional theory (DFT), have been extensively used to determine reaction barriers thus shedding light on possible reaction mechanisms.[7-10] Similarly, DFT calculations have been employed to identify trends across different acid sites.[11-17]

The focus of the vast majority of these theoretical studies has so far been directed towards Brønsted acid sites (BAS) inside the porous zeolite. For BAS, a tetrahedrally coordinated silicon atom is substituted by an aluminum atom, introducing a proton for charge balance (see Scheme 1). Depending on temperature and partial pressures, oxygenates such as water, methanol and dimethyl ether (DME) adsorb at the BAS through formation of a hydrogen bond. Recent studies also focus on aluminum siting[18-20] as well as the effect of different Si/Al ratios.[21-24] The reactivity of surface BAS, however, has rarely been studied, although with a crystal size of a few nanometers to micrometers,[25-26] zeolite particles as well as 2D-zeolites[27-31] offer a large surface area. At the surface, substitution of a silicon atom at a single silanol group followed by dehydration leads to a three-fold coordinated aluminum atom (a structural motif not present in BAS sites), which generally acts as a Lewis acid site (LAS, see Scheme 1). The existence of a three-fold coordinated aluminum atom in the zeolite framework, including also the position at the surface, as a reactive intermediate has been investigated in both theoretical and experimental studies.[32-39] As for the BAS, adsorption of water, methanol and DME can occur at LAS. The oxygenates bind as Lewis bases directly to the Al-atom, which is then four-fold coordinated. Water adsorption occurs at ambient conditions and has been studied in detail by Chizallet and coworkers for H-ZSM-5.[36] Other structural motifs leading to LAS are extraframework aluminum[40-44] and substitution of zeolites with elements such as Sn or Zn.[45-48] The influence of LAS on reaction mechanisms in the MTO process

has been discussed,[49-53] but computational explorations are still scarce. They exist, however, for other reactions, such as the tautomerization of phenol and catechol[35] or the deoxygenation of methyl butyrate.[54]

In this work, we investigate the reactivity of acid sites introduced by aluminum substitution at the surface of H-SSZ-13 giving rise to both BAS and LAS. Our goal is to compare the reactivity of surface BAS with those in the bulk by considering the four different oxygen atoms adjacent to the aluminum substitution. Furthermore, we aim at gaining fundamental insights into the reactivity of surface LAS in particular in comparison to their BAS counterpart. We use the formation of DME from methanol (MeOH) as an important probe reaction that captures the typical reactivity of BAS.[55-56]

COMPUTATIONAL DETAILS:

The studied catalyst H-SSZ-13 crystalizes in the chabazite structure. The lattice constants were optimized in earlier work to 13.625, 13.625, and 15.067 Å.[7] The initial bulk structure containing only one unique T-site has a Si/Al ratio of 35:1. The surface structures were built by terminating the repeated bulk structures at the facets. Afterwards, broken bonds were saturated as silanol groups. For each BAS, the stepwise mechanism was investigated at all four oxygen atoms adjacent to the aluminum atom (see SI section 10 for details). In the main manuscript, the systems with the lowest energy barriers were discussed only.

Structure optimizations were carried out with periodic DFT using the dispersion-corrected functional PBE-D3 [57-58] and a convergence criterion of 0.001 eV/Å. The projector-augmented-wave method and an energy cutoff of 400 eV were applied using the Vienna Ab initio Simulation Package (VASP) in version 5.4.1[59-60] along with the Atomic Simulation Environment (ASE).[61] Vibrations were calculated by computing a partial Hessian consisting of the adsorbate atoms and the active site of the catalyst, which includes the Al atom and the surrounding O and Si atoms, i.e., three OSi units for LAS and four OSi units for BAS. Free energies were calculated with the harmonic-oscillator approximation and for gas phase molecules additionally with the rigid-rotator and the free-translator approximation were applied. Frequencies below 12 cm^{-1} were raised to this value to avoid larger inaccuracies of the entropies due to the harmonic-oscillator approximation. Transition state searches were performed using Automated Relaxed Potential Energy Surface Scan (ARPESS).[62] The connectivity of transition states was verified through distortion along the normal mode followed by optimization towards the endpoints.

Since DFT calculations underestimate transition state energies, [63] single-point calculations of cluster models were applied to obtain energy correction terms $\Delta E^{\text{cluster}}$ (see Eq. (1) and Eq. (2)):[64]

$$\Delta E^{\text{cluster}} = E^{\text{cluster}}_{\text{DLPNO-CCSD(T)/DZ}} + \Delta E^{\text{cluster}}_{\text{MP2/CBS}} - E^{\text{cluster}}_{\text{PBE-D3}} \qquad (1)$$

$E^{\text{cluster}}_{\text{DLPNO-CCSD(T)/DZ}}$ is the DLPNO-CCSD(T) energy, $E^{\text{cluster}}_{\text{PBE-D3}}$ is the DFT energy, and $\Delta E^{\text{cluster}}_{\text{MP2/CBS}}$ is the correction for the CBS extrapolation. The latter includes Hartree-Fock (HF) and MP2 correlation separately extrapolated with cc-pVDZ, cc-pVTZ, and cc-pVQZ using the three-point exponential fit[49] and cc-pVDZ and cc-pVTZ using the two-point X^{-3} fit,[50] respectively. The program package ORCA[65] was used for HF, MP2, and CCSD(T) calculations. For CCSD(T) and MP2, the cc-pVDZ and cc-pVXZ basis sets[66] with X = D, T were used, respectively. The DLPNO approximation was applied, using the "TightPNO" threshold setting.[67-69] For HF calculations, the cc-pVXZ basis sets with X = D, T, Q and the RIJCOSX approximation[70] with GridX6 were used. For non-periodic DFT calculations, the PBE-D3 functional, the def2-TZVPP basis set[71-72], and the resolution of identity approximation[73] implemented in the program package TURBOMOLE[74] were used. The cluster models for BAS1(001), BAS2(001), and LAS1(001) have 52 T-sites and the cluster model for LAS2(001) has 39 T-sites. All cluster models for the (101) terminations have 64 T-sites, those for the bulk have 36 T-sites. The Cartesian coordinates of these structures are provided in the SI.

Scheme 1: Illustration of a Brønsted acid site (BAS) and a surface Lewis acid site (LAS). Adsorption of H_2O, methanol or DME is computed to be favorable at 200 °C and 1 bar partial pressure and generally depends on the external conditions.

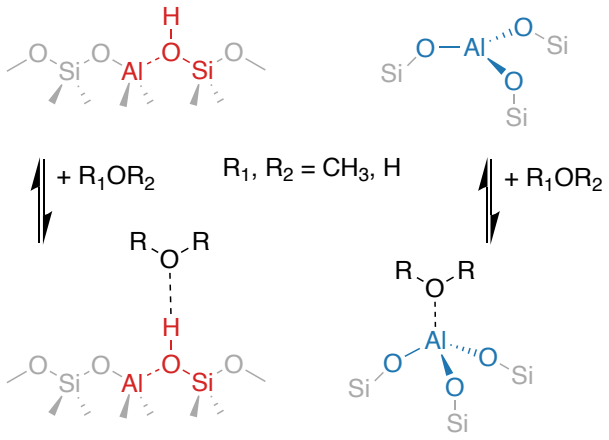

RESULTS AND DISCUSSION:

In our computational investigation, we employ periodic DFT optimizations at the PBE-D3 level[57-58] and compute Gibbs free energies at a reference pressure of 1 bar using the harmonic approximation as well as the rigid-rotator and free-translator approximation for gas phase molecules. This pressure is within the range of settings used in experimental MTO studies and DME syntheses. [3-4, 56, 75-76] The energies are corrected using single point energy calculations on cluster models, as described in previous work.[64] We employ complete basis set (CBS)-extrapolated DLPNO-MP2 calculations and account for the difference between DLPNO-CCSD(T) and DLPNO-MP2 at the cc-pVDZ level of theory. The Gibbs free energy is then simply computed as:

$$G = E^{\text{PBC}}_{\text{PBE-D3}} + \Delta E^{\text{cluster}} + \Delta G^{\text{PBC}}_{\text{harm}} \qquad (2)$$

Here, $E^{\text{PBC}}_{\text{PBE-D3}}$ is the DFT energy computed for periodic models, $\Delta E^{\text{cluster}}$ is the energy correction derived from the cluster models (see Section Computational Details), and $\Delta G^{\text{PBC}}_{\text{harm}}$ are the harmonic contributions derived from normal mode analysis. Choosing representative conditions for

the DME synthesis and the MTO process, we considered temperatures of 200 °C and 400 °C.

STABILITY OF H-SSZ-13 SURFACE TERMINATIONS:

Chizallet and coworkers studied aluminum substitutions on the (100), (010) and (101) surfaces of the H-ZSM-5 zeolite and on the (001) surface of the BETA zeolite. [36, 77-79] The presence of several T-sites and multiple possible surface terminations lead to various potential aluminum surface sites. By comparing formation energies, Chizallet and coworkers found that substitution of aluminum into the surface is often more stable than its position in the bulk. This means that there is a driving force for the formation of these aluminum surface sites.

We employ similar substitutions as those introduced by Chizallet and coworkers using surface terminations of the H-SSZ-13 crystal due to its simple structure. It crystallizes in the chabazite framework type (CHA), which contains only one unique T-site, reducing the number of potential surface sites compared to, e.g., H-ZSM-5. The crystals of H-SSZ-13 and some other zeolites with CHA structure, such as H-SAPO-34, commonly have a cubic or almost cubic form.[25, 80-81] While the shape of the crystals is known, the surface orientations have – to the best of our knowledge – been sparsely investigated. Based on the CHA-structure and the common finding that low-index facets are often most stable,[36] we initially investigated the (101), (110), (001), and (100) surfaces, focusing on purely silicious surfaces to determine their stability. For the (100) and (101) surfaces, two equivalent surfaces exist, the (010) and ($\bar{1}$10) surfaces and the ($\bar{1}$11) and (0$\bar{1}$1) surfaces, respectively. We found the surface free energies γ of the investigated structures to be very similar at low temperatures (Fig. 1a), with their differences increasing with increasing temperature. These differences can largely be attributed to the number of Si-O-Si-bonds that have to be broken at the surface under formation of silanol groups (Si-OH) (see Fig. 1b). The formation of silanol groups requires the reaction with water, which becomes increasingly less favorable with increasing temperature for entropic reasons, while it is almost thermoneutral at 0 K. We find that the (101) surface requires the least amount of broken Si-O-Si bonds and is therefore most stable at high temperatures.

Crystals with CHA framework were reported to terminate with the (101) facet in an almost cubic shape,[82-83] which is in agreement with a Wulff construction (Fig. 1) based on this surface termination. This, as well as its low surface free energy, makes the (101) facet the most likely surface termination and we therefore studied this surface in detail. We additionally considered the previously studied (001) facet[84] to investigate to which extent the reactivity depends on the specific surface orientation.

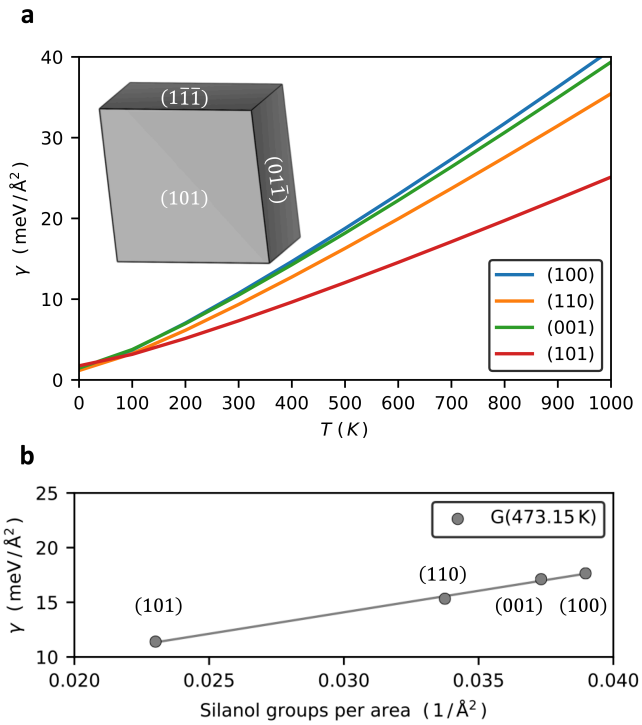

Figure 1. a) Surface free energies γ as a function of temperature for the silicious (100), (111), (001), and (101) facets and the Wulff construction using the (101) and symmetry-equivalent facets. b) Dependence of the stabilities of silicious facets on the number of silanol groups per area at 200 °C.

CHARACTERIZATION OF H-SSZ-13 SURFACE ACID SITES:

Figure 2 shows the atomic structure of the (101) facet of H-SSZ-13, which is terminated in the way that requires least Si-O-Si bond breaking. In this termination, the double-six rings are left intact and the eight-membered rings orthogonal to the surface are cut in half. Figure 2 also shows the possible aluminum substitutions. Substituting a silicon at a silanol group with aluminum leads to a LAS, which we label LAS1(101). Substituting a silicon without a silanol group by aluminum leads to a BAS. We label this kind of substitutions BAS1(101) and BAS2(101), respectively. In addition, we considered the BAS in the bulk unit cell, labeled BASB. The structure and corresponding substitutions belonging to the (001) facet of SSZ-13 are shown in Figure S1.

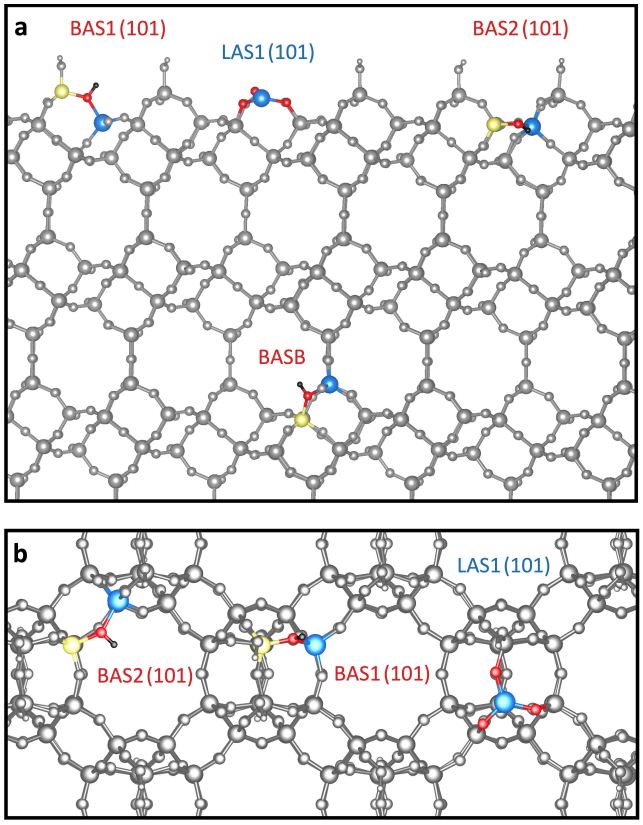

Figure 2. a) Side view and b) top view of the of SSZ-13 (101) structure. The different LAS and BAS studied in this work are indicated. Color code: Grey: Framework, Blue: Aluminum, Yellow: Silicon, Red: Oxygen, Black: Hydrogen, Brown: Carbon, Green: Nitrogen.

Experimentally, LAS and BAS can be distinguished through infrared spectroscopy of adsorbed probe molecules. The most commonly used probe molecule for the identification of LAS is pyridine (see Fig. 3). Here, the 19b vibration is typically blueshifted by 5 to 20 cm^{-1} for LAS and 90 to 110 cm^{-1} for adsorption at a BAS, thus resulting in a difference of approximately 70 to 115 cm^{-1} between adsorption on the two different sites.[85-88] We reproduced this behavior also in our calculations, with blueshifts for LAS around 16 to 17 cm^{-1} and for BAS around 114 to 125 cm^{-1} with differences in the range of 96 to 109 cm^{-1} (Table 1).

For BAS, all four oxygen atoms adjacent to the aluminum were investigated. The most stable structures at 200°C are discussed only.

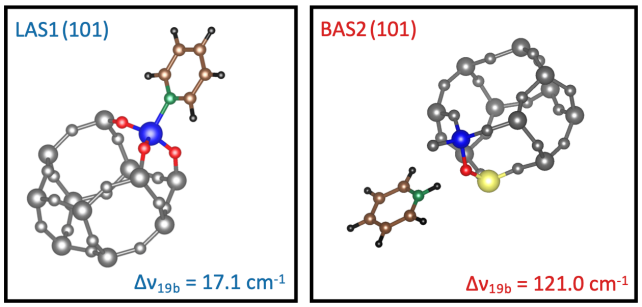

Figure 3. Calculated structures of adsorbed pyridine at a LAS and a BAS and corresponding shifts of the computed harmonic frequencies of the 19b mode relative to molecule in the gas phase.

Table 1. Computed vibrational harmonic frequencies of the 19b mode of pyridine and vibrational shifts relative to pyridine in the gas phase.

System	19b Frequency (cm^{-1})
gas phase	1427.0 (exp: 1440)[89]
LAS1 (101)	1444.1 ($\Delta\nu$ = 17.1)
LAS1 (001)	1444.8 ($\Delta\nu$ = 17.8)
LAS2 (001)	1443.6 ($\Delta\nu$ = 16.6)
BAS1 (101)	1552.2 ($\Delta\nu$ = 125.2)
BAS2 (101)	1548.0 ($\Delta\nu$ = 121.0)
BAS1 (001)	1552.0 ($\Delta\nu$ = 125.0)
BAS2 (001)	1543.2 ($\Delta\nu$ = 116.2)
BASB	1540.8 ($\Delta\nu$ = 113.8)

In order to assess the relevance of the discussed sites, we computed the relative stability with respect to the reference bulk structure for several temperatures, also taking adsorption of water and MeOH for all sites into account (Figs. S2 and S3). The BAS in the bulk and in various surface positions differ by less than 16 kJ/mol in stability. Considering only water adsorbed systems, their stabilities differ by less than 6 kJ/mol. To discuss the stability of LAS, it is important to consider the difference in the amount of adsorbed water. When a bulk Si atom is substituted by Al, a proton is introduced for charge balance. On the other hand, substituting a Si atom at a silanol group requires to remove the OH to obtain a clean LAS. Consequently, a clean BAS and a clean LAS differ by one water molecule. This also means that a BAS with a single adsorbed H_2O contains one more H_2O molecule than a LAS with a single adsorbed H_2O. This generally favors LAS entropically and we find that – in the presence of water – LAS are of similar or higher stability than BAS for T > 300 K (see Fig. S3). This relatively high stability of Al substituted on the surface of porous materials has already been reported by Chizallet[36] and coworkers. Although we note that, experimentally, the distribution of Al atoms is controlled by the synthesis process and not necessarily by the stability under the discussed conditions, the calculations certainly indicate that these sites are reasonably stable and likely to be present for these catalytic systems.

Table 2 lists the calculated adsorption energies of Lewis basic adsorbates, which are generally more strongly adsorbed on LAS than on BAS. The ordering of adsorption energies, from weakest to strongest, is H_2O^* < DME* ≈ MeOH* < pyridine*. The adsorption energies of water, methanol, and DME are similar for the different BAS, while larger differences are observed for LAS. The obtained adsorption energies for pyridine are comparable to those from other computational studies for chabazite surface BAS ($\Delta E_{Ad,\ pyridine}$ = 130 to 181 kJ/mol). [90]

Table 2. Computed zero-point vibrational-energy corrected adsorption energies ΔE_{Ad} in kJ/mol.

	H_2O*	MeOH*	DME*	pyridine*
LAS1(101)	-126	-148	-163	-194
LAS1(001)	-135	-158	-169	-205
LAS2(001)	-133	-154	-143	-185
BAS1(101)	-67	-82	-79	-165
BAS2(101)	-74	-86	-87	-173
BAS1(001)	-80	-83	-88	-171
BAS2(001)	-74	-90	-84	-170
BASB	-75	-91	-90	-177

REACTIVITY OF H-SSZ-13 SURFACE ACID SITES:

Next, we focus on the reactivity of the various acid sites, taking the dehydration reaction of MeOH to DME as an example, as it has been investigated extensively, both experimentally and theoretically.[19, 55, 76, 91-95] Furthermore, this reaction exhibits many similarities to other methylation reactions that can occur in zeolites, for example the methylation of olefins and aromatic molecules.[96-103]

There are two commonly accepted mechanisms for DME formation on a BAS: The stepwise (also called dissociative, Fig. 4a) and the concerted (also called associative, Fig. 5a) mechanism. In the stepwise mechanism, DME is formed through reaction of a surface methoxy species (SMS) with MeOH. In the concerted mechanism, two adsorbed MeOH react directly. Due to the higher entropic penalty of the concerted mechanism, the stepwise mechanism typically contributes more to the overall reaction rate at higher temperatures.[19, 76, 104] We start by analyzing our calculations of the stepwise mechanism on BAS (Fig. 4). The SMS is created after protonation of methanol, where the protonated methanol rotates and transfers its methyl group to the acid site, liberating water (TS-s1). After water desorption, this methyl group is transferred to the second MeOH, forming protonated DME (TS-s2). Protonation reactions of DME and methanol were neglected in all our calculations as their energy barriers are expected to be low. For methanol, this was explicitly calculated previously.[105] Figure 4b compares the free energy diagram of the stepwise mechanism for three different BAS, i.e., located in the bulk and on the (001) (denoted BAS1(001)) and (101) (denoted BAS2(101)) surface, at a temperature of 200 °C and 1 bar reference pressures. As can be seen, the adsorption energies of methanol and DME (see also Table 2) as well as the transition state energies (see also Table 3) are fairly similar. Table 2 shows a maximum difference of MeOH and DME adsorption energies at BAS of 11 kJ/mol referenced to the BASB. Table 3 shows a maximum difference of energy barriers for BAS of 14 kJ/mol referenced to the BASB. The small deviations in acid site reactivity are also observed in the calculated pyridine adsorption energies, differing by a maximum of 12 kJ/mol between the BAS (see Table 2). Similar differences have been observed for adsorption of ammonia on the twelve different BAS within H-ZSM-5.[21]

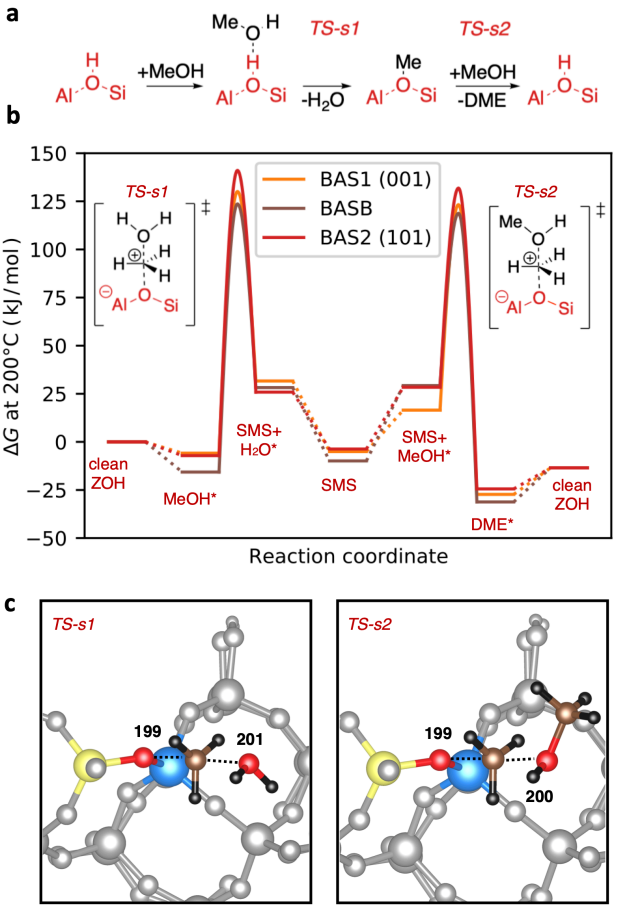

Figure 4. a) Stepwise mechanism. b) Free energy diagrams for BAS1(001), BAS2(101), and BASB at 200 °C and 1 bar. c) Computed transition state structures for BAS2(101) with bond lengths indicated in pm.

We now turn to analyzing the concerted mechanism, where LAS will also be discussed. Since water adsorbed LAS is energetically favored significantly over the clean system, it is included in Fig. 5. Starting with the surface BAS BAS2(101) an adsorbed MeOH reacts directly with a second MeOH in a concerted mechanism (Fig. 5a). This reaction proceeds via an S_N2-mechanism, where the methyl group is transferred from the protonated methanol to the second methanol (TS-cB), resulting in the formation of water and protonated DME, which is then readily deprotonated to give the final products, DME and water. The overall free energy barrier from adsorbed methanol to the transition state is calculated to 155 kJ/mol for BAS2(101) at 200 °C and 1 bar. This is slightly higher than the overall free energy barrier obtained for the stepwise mechanism at the same BAS ($\Delta G^{200°C}$=148 kJ/mol, see Figure 4b). Our calculations thus suggest that the stepwise mechanism dominates at these reaction conditions, in line with earlier theoretical work.[76, 104]

For a LAS, an analogous mechanism, resembling the concerted mechanism on a BAS, can be formulated. This is exemplified for the LAS1(101) in Figure 5b, compared to the BAS counterpart, also using the (101) surface termination. The desorption of water is discussed in SI section S5. Starting from a clean LAS, MeOH adsorbs at the LAS. Notably,

methanol adsorption is stronger by 60 kJ/mol compared to the adsorption at a BAS (see also Table 2). DME formation now proceeds via transfer of the methyl group in an S_N2-mechanism to a second methanol (TS-cL). This results in the formation of a protonated DME and a negatively charged framework with an Al-OH group (iso-electronic to a silanol group). Deprotonation yields free DME and an acid site with a coordinatively bound water molecule (see Fig. 5). Interestingly, the calculated free energy barrier for the LAS is of similar height compared to the BAS when referenced to adsorbed methanol ($\Delta G^{\ddagger}$ at 200 °C of 157 kJ/mol for LAS1(101) vs. 155 kJ/mol for BAS2(101), see Fig. 5b). The concerted mechanisms on the BAS and LAS are thus rather similar, but differ such that all intermediates and transition states are about 60 kJ/mol lower in free energy for the LAS. From a kinetic point of view, one would therefore assume that the reaction rate, starting from adsorbed methanol, is similar when comparing the two Brønsted and Lewis acid sites. Due to the much stronger adsorption of the products, H_2O and DME, at LAS one would expect product and/or water poisoning to a much larger extend for the LAS, decreasing the overall activity.

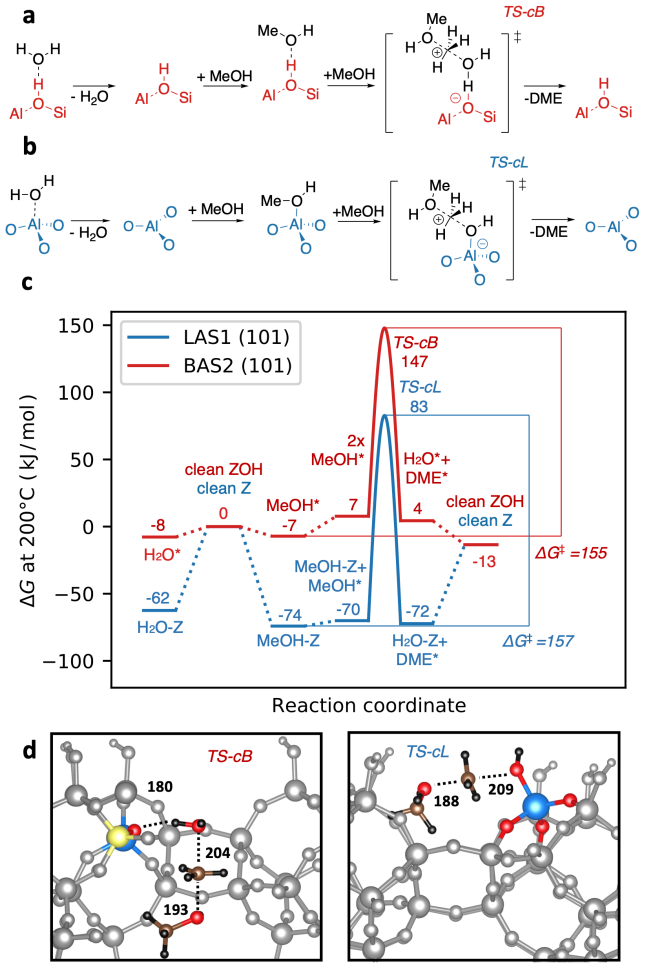

Figure 5. a) Concerted mechanism at BAS. b) Mechanism at LAS. c) Free energy diagrams at 200 °C for BAS2(101) and LAS1(101). d) Computed transition state structures with bond lengths indicated in pm.

We now investigate the similarities and differences between these two acid sites in more detail. At a BAS, for the TS-cB, the two protonated MeOH in the direct TS are only loosely bound to the framework via hydrogen bonds. For the LAS, on the other hand, the oxygen of the initially adsorbed methanol remains strongly bound to the Al atom of the acid site throughout the reaction. In TS-cL the Al-O distance to the oxygen of the adsorbed MeOH is 181 pm, which is comparable to the average Al-O distance of the other three Al-O bonds (174 pm). The final product water remains strongly bound (binding energy -126 kJ/mol, see Table 2).

We calculated the reaction barriers for the stepwise and concerted mechanism on all BAS and LAS sites investigated herein. These are given in Table 3 and Figure S7 (200 °C), and Table S3 and Figure S7 (400 °C). Note that these barriers are always referenced to the most stable initial states [106] as illustrated in Figure 5c for the concerted mechanism. At 200 °C, the most stable state is generally a single adsorbed MeOH molecule for TS-cL, TS-s1, and TS-cB. Depending on the system, adsorbed methanol or SMS is more stable. For improved comparability, we use SMS as the reference of TS-s2 for all systems. First, we discuss the free energy barriers at 200 °C, which is in the typical temperature range for zeolite-catalyzed DME formation.[56, 107-108] We find that, for the BAS, the ordering of the barriers is mostly the same, i.e., TS-cB > TS-s1 > TS-s2. The only exception is BAS2(001), where TS-s1 has a lower energy barrier than TS-s2, when referenced to methanol instead of SMS (see Fig. S6 and Table S1). The barriers for the various BAS do not differ significantly from the bulk site, BASB, with mean absolute deviations of 6 kJ/mol, 9 kJ/mol, and 7 kJ/mol for TS-s1, TS-s2, and TS-cB, respectively. With values of 157 to164 kJ/mol, the barriers for DME formation at LAS (TS-cL) are similar to those of the concerted mechanism at BAS (TS-cB), as also observed in Figure 5c.

We also investigated the barriers at 400 °C, as this temperature is more typical for MTO-type reactions, and similar methylation reactions play a major role for these processes. [8, 97-98, 109-110] At 400 °C, the initial state is still SMS for TS-s2 and a single adsorbed MeOH for TS-cL, but it is generally the clean acid site and MeOH in the gas phase for both TS-cB and TS-s1. This is due to the increased entropy loss for adsorbed intermediates at higher temperatures and the stronger binding at LAS. Consequently, the activation free energy for the concerted mechanism is at least 38 kJ/mol higher than that for the stepwise mechanism for all BAS (Fig. S7). Considering the different energy contributions, it is worth noting that PBE-D3 generally underestimates the transition state energy of the concerted mechanism by about 40 kJ/mol, while the transition states of the stepwise mechanism are underestimated only by about 20 kJ/mol (both deviations are referenced to clean BAS).

Table 3. Gibbs free energy barriers in kJ/mol, referenced to the active site with one adsorbed MeOH for TS-s1, TS-cB, and TS-cL, and to the clean SMS for TS-s2 at 200 °C and 1 bar. Barriers at 400 °C are given in Table S3.

	concerted	stepwise	
	TS-cB / TS-cL	TS-s1	TS-s2
BASB	162	139	129
BAS1(001)	158	136	128
BAS2(001)	151	128	123
BAS1(101)	165	153	141
BAS2(101)	155	148	136
LAS1(001)	164		
LAS2(001)	162		
LAS1(101)	157		

Finally, we note that a H_2O or MeOH molecule adsorbed on a LAS has also been shown to be able to act as a BAS.[36] For the formation of DME from methanol, however, mechanisms utilizing these Brønsted acidic adsorbed molecules are intrinsically unfavorable entropically. For example, a stepwise mechanism initiated by adsorbed H_2O contains the same number of molecules as the concerted mechanism mediated by adsorbed methanol discussed above. We studied some of these mechanisms explicitly and found them to be less favorable with barriers that are higher by about 50 kJ/mol (see SI).

CONCLUSIONS:

We investigated several surfaces of H-SSZ-13 and found that their stability is mainly determined by the number of silanol groups per surface area. We further explored aluminum substitution at the (001) and the (101) facet, the latter being the most stable surface. Brønsted acid sites in the bulk and in different surface positions were found to be very similar in stability, differing by up to 10 kJ/mol. Clean Lewis acid sites contain one water molecule less than clean Brønsted acid sites and become increasingly more stable at temperatures above 400 °C, where adsorption of methanol and water becomes unfavorable at both sites. Additionally, adsorption of water is 57 kJ/mol stronger on Lewis acid sites considering the difference between the MAE of the adsorption energies of Brønsted and Lewis acid sites. For this reason, Lewis acid sites are also more stable in presence of adsorbates in the intermediate temperature range between 200 °C and 400 °C.

The dehydration of methanol to DME was studied as a probe reaction at both Lewis and Brønsted acid sites. We found the energy barriers catalyzed by Brønsted acid sites to be similar at the surface and in the bulk, with small differences of only 7 kJ/mol. DME formation catalyzed by Lewis acid sites occurs through the reaction of two adsorbed methanol molecules. This mechanism is thus similar to the concerted (associative) mechanism known for Brønsted acid sites. Interestingly, we also found that the barriers are comparable, being on the order of 160 kJ/mol at 200 °C. Since the stepwise mechanism at Brønsted acid sites is computed to be slightly more favorable already at 200 °C, DME formation at Lewis acid sites occurs with barriers that are generally less favorable by 2 to 36 kJ/mol, depending on the specific site. In addition, product and/or water poisoning is expected to be more problematic for LAS, since adsorption is significantly stronger than on BAS.

Based on these observations, we therefore conclude that LAS play a minor role in the dehydration of methanol to DME and contribute even less to the rate of methylation reactions at higher temperatures, as, e.g., occurring in the MTO process. The similarities between LAS and BAS for the concerted mechanism are striking, both with respect to energies of transition states and their corresponding geometries, and we therefore speculate that LAS might contribute to reactions dominated by a concerted methylation mechanism where poisoning of active sites is unproblematic.

AUTHOR INFORMATION

Corresponding Author

Philipp N. Plessow – *Institute of Catalysis Research and Technology, Karlsruhe Institute of Technology, Eggenstein-Leopoldshafen 76344, Germany; orcid.org/0000-0001-9913-4049; Email: philipp.plessow@kit.edu*

Authors

Philipp Huber – *Institute of Catalysis Research and Technology, Karlsruhe Institute of Technology, Eggenstein-Leopoldshafen 76344, Germany; orcid.org/0000-0001-6862-8177*

Felix Studt – *Institute of Catalysis Research and Technology and Institute for Chemical Technology and Polymer Chemistry, Karlsruhe Institute of Technology, Eggenstein-Leopoldshafen 76344, Germany; orcid.org/0000-0001-6841-4232*

Author Contributions

The manuscript was written through contributions of all authors. All authors have given approval to the final version of the manuscript.

Notes

The authors declare no competing financial interests.

ASSOCIATED CONTENT

Supporting Information

The Supporting Information is available free of charge on the ACS Publications website.

Detailed information regarding the stability of the surfaces and active sites, data of additional reaction mechanisms, detailed data for the concerted and stepwise mechanisms at all active sites, additional information about the studied structures, total energies, and vibrational modes (PDF).

Studied structures in POSCAR and XYZ format (ZIP)

ACKNOWLEDGMENTS

The authors acknowledge support by the state of Baden-Württemberg through bwHPC (bwunicluster and JUSTUS, RV bw17D011). Financial support from the Helmholtz Association is also gratefully acknowledged. Gefördert durch die Deutsche Forschungsgemeinschaft (DFG) – Projektnummer 434253773.

REFERENCES

1. Van Speybroeck, V.; Hemelsoet, K.; Joos, L.; Waroquier, M.; Bell, R. G.; Catlow, C. R., Advances in Theory and Their Application within the Field of Zeolite Chemistry. *Chem. Soc. Rev.* **2015**, *44*, 7044-7111.
2. Perego, C.; Bosetti, A.; Ricci, M.; Millini, R., Zeolite Materials for Biomass Conversion to Biofuel. *Energy & Fuels* **2017**, *31*, 7721-7733.
3. Olsbye, U.; Svelle, S.; Bjorgen, M.; Beato, P.; Janssens, T. V.; Joensen, F.; Bordiga, S.; Lillerud, K. P., Conversion of Methanol to Hydrocarbons: How Zeolite Cavity and Pore Size Controls Product Selectivity. *Angew. Chem. Int. Ed. Engl.* **2012**, *51*, 5810-5831.
4. Stöcker, M., Methanol-to-Hydrocarbons: Catalytic Materials and Their Behavior. *Microporous Mesoporous Mater.* **1999**, *29*, 3-48.
5. Hemelsoet, K.; Van der Mynsbrugge, J.; De Wispelaere, K.; Waroquier, M.; Van Speybroeck, V., Unraveling the Reaction Mechanisms Governing Methanol-to-Olefins Catalysis by Theory and Experiment. *ChemPhysChem* **2013**, *14*, 1526-1545.
6. Van Speybroeck, V.; De Wispelaere, K.; Van der Mynsbrugge, J.; Vandichel, M.; Hemelsoet, K.; Waroquier, M., First Principle Chemical Kinetics in Zeolites: The Methanol-to-Olefin Process as a Case Study. *Chem. Soc. Rev.* **2014**, *43*, 7326-7357.
7. Plessow, P. N.; Studt, F., Unraveling the Mechanism of the Initiation Reaction of the Methanol to Olefins Process Using Ab Initio and DFT Calculations. *ACS Catal.* **2017**, *7*, 7987-7994.
8. Brogaard, R. Y.; Henry, R.; Schuurman, Y.; Medford, A. J.; Moses, P. G.; Beato, P.; Svelle, S.; Nørskov, J. K.; Olsbye, U., Methanol-to-Hydrocarbons Conversion: The Alkene Methylation Pathway. *J. Catal.* **2014**, *314*, 159-169.
9. Wang, C.-M.; Wang, Y.-D.; Xie, Z.-K., Verification of the Dual Cycle Mechanism for Methanol-to-Olefin Conversion in HSAPO-34: A Methylbenzene-Based Cycle from DFT Calculations. *Catal. Sci. Technol.* **2014**, *4*, 2631-2638.
10. Wang, C.-M.; Wang, Y.-D.; Du, Y.-J.; Yang, G.; Xie, Z.-K., Computational Insights into the Reaction Mechanism of Methanol-to-Olefins Conversion in H-ZSM-5: Nature of Hydrocarbon Pool. *Catal. Sci. Technol.* **2016**, *6*, 3279-3288.
11. Brogaard, R. Y.; Wang, C.-M.; Studt, F., Methanol–Alkene Reactions in Zeotype Acid Catalysts: Insights from a Descriptor-Based Approach and Microkinetic Modeling. *ACS Catal.* **2014**, *4*, 4504-4509.
12. Wang, C. M.; Brogaard, R. Y.; Weckhuysen, B. M.; Norskov, J. K.; Studt, F., Reactivity Descriptor in Solid Acid Catalysis: Predicting Turnover Frequencies for Propene Methylation in Zeotypes. *J. Phys. Chem. Lett.* **2014**, *5*, 1516-1521.
13. Wang, C.-M.; Brogaard, R. Y.; Xie, Z.-K.; Studt, F., Transition-State Scaling Relations in Zeolite Catalysis: Influence of Framework Topology and Acid-Site Reactivity. *Catal. Sci. Technol.* **2015**, *5*, 2814-2820.
14. Liu, C.; Tranca, I.; van Santen, R. A.; Hensen, E. J. M.; Pidko, E. A., Scaling Relations for Acidity and Reactivity of Zeolites. *J. Phys. Chem. C* **2017**, *121*, 23520-23530.
15. Wang, C.-M.; Wang, Y.-D.; Xie, Z.-K., General Scaling Relations and Prediction of Transition State Energies in CHA/ALPO-34-Structured Zeolite Catalysis Related to the Methanol-to-Olefins Conversion. *Catal. Sci. Technol.* **2019**, *9*, 2245-2252.
16. Plessow, P. N.; Studt, F., How Accurately Do Approximate Density Functionals Predict Trends in Acidic Zeolite Catalysis? *J. Phys. Chem. Lett.* **2020**, *11*, 4305-4310.
17. DeLuca, M.; Janes, C.; Hibbitts, D., Contrasting Arene, Alkene, Diene, and Formaldehyde Hydrogenation in H-ZSM-5, H-SSZ-13, and H-SAPO-34 Frameworks During MTO. *ACS Catal.* **2020**, 4593-4607.
18. Ghorbanpour, A.; Rimer, J. D.; Grabow, L. C., Periodic, vdW-Corrected Density Functional Theory Investigation of the Effect of Al Siting in H-ZSM-5 on Chemisorption Properties and Site-Specific Acidity. *Catal. Commun.* **2014**, *52*, 98-102.
19. Ghorbanpour, A.; Rimer, J. D.; Grabow, L. C., Computational Assessment of the Dominant Factors Governing the Mechanism of Methanol Dehydration over H-ZSM-5 with Heterogeneous Aluminum Distribution. *ACS Catal.* **2016**, *6*, 2287-2298.
20. Smith, A. T.; Plessow, P. N.; Studt, F., Effect of Aluminum Siting in H-ZSM5 on Reaction Barriers. *J. Phys. Chem. C* **2021**.
21. Smith, A. T.; Plessow, P. N.; Studt, F., Trends in the Reactivity of Proximate Aluminum Sites in H-SSZ-13. *J. Phys. Chem. C* **2021**, *125*, 16508-16515.
22. Lopez-Orozco, S.; Inayat, A.; Schwab, A.; Selvam, T.; Schwieger, W., Zeolitic Materials with Hierarchical Porous Structures. *Adv. Mater.* **2011**, *23*, 2602-2615.
23. Valtchev, V.; Majano, G.; Mintova, S.; Perez-Ramirez, J., Tailored Crystalline Microporous Materials by Post-Synthesis Modification. *Chem. Soc. Rev.* **2013**, *42*, 263-290.
24. Dědeček, J.; Sklenak, S.; Li, C.; Wichterlová, B.; Gábová, V.; Brus, J.; Sierka, M.; Sauer, J., Effect of Al-Si-Al and Al-Si-Si-Al Pairs in the ZSM-5 Zeolite Framework on the ^{27}Al NMR Spectra. A Combined High-Resolution ^{27}Al NMR and DFT/MM Study. *J. Phys. Chem. C* **2009**, *113*, 1447-1458.
25. He, Y.-R.; Zhu, Y.-L.; Duan, Y.; Zhang, M.; Jiang, J., Green Route to Grow Hierarchical SAPO-34 Crystal with Excellent Catalytic Performance in Methanol to Olefin Reaction. *Cryst. Growth Des.* **2019**, *20*, 17-23.
26. Li, Z.; Navarro, M. T.; Martínez-Triguero, J.; Yu, J.; Corma, A., Synthesis of Nano-SSZ-13 and Its Application in the Reaction of Methanol to Olefins. *Catal. Sci. Technol.* **2016**, *6*, 5856-5863.
27. Rybicki, M.; Sauer, J., Acidity of Two-Dimensional Zeolites. *Phys. Chem. Chem. Phys.* **2015**, *17*, 27873-27882.
28. Sauer, J., Bronsted Activity of Two-Dimensional Zeolites Compared to Bulk Materials. *Faraday Discuss.* **2016**, *188*, 227-234.
29. Thang, H. V.; Rubes, M.; Bludsky, O.; Nachtigall, P., Computational Investigation of the Lewis Acidity in Three-Dimensional and Corresponding Two-Dimensional Zeolites: UTL Vs IPC-1P. *J. Phys. Chem. A* **2014**, *118*, 7526-7534.
30. Ho, T. V.; Nachtigall, P.; Grajciar, L., The Lewis Acidity of Three- and Two-Dimensional Zeolites: The Effect of Framework Topology. *Catal. Today* **2018**, *304*, 12-21.
31. Thang, H. V.; Vaculík, J.; Přech, J.; Kubů, M.; Čejka, J.; Nachtigall, P.; Bulánek, R.; Grajciar, L., The Brønsted Acidity of Three- and Two-Dimensional Zeolites. *Microporous Mesoporous Mater.* **2019**, *282*, 121-132.
32. Brus, J.; Kobera, L.; Schoefberger, W.; Urbanova, M.; Klein, P.; Sazama, P.; Tabor, E.; Sklenak, S.; Fishchuk, A. V.; Dedecek, J., Structure of Framework Aluminum Lewis Sites and Perturbed Aluminum Atoms in Zeolites as Determined by ^{27}Al{^{1}H} REDOR (3Q) MAS NMR Spectroscopy and DFT/Molecular Mechanics. *Angew. Chem. Int. Ed. Engl.* **2015**, *54*, 541-545.
33. Ravi, M.; Sushkevich, V. L.; van Bokhoven, J. A., Lewis Acidity Inherent to the Framework of Zeolite Mordenite. *J. Phys. Chem. C* **2019**, *123*, 15139-15144.
34. van Bokhoven, J. A.; Van der Eerden, A. M.; Koningsberger, D. C., Three-Coordinate Aluminum in Zeolites Observed with in Situ X-Ray Absorption near-Edge Spectroscopy at the Al K-Edge: Flexibility of Aluminum Coordinations in Zeolites. *J. Am. Chem. Soc.* **2003**, *125*, 7435-7442.
35. Hernandez-Tamargo, C. E.; Roldan, A.; de Leeuw, N. H., Density Functional Theory Study of the Zeolite-Mediated Tautomerization of Phenol and Catechol. *Mol. Catal.* **2017**, *433*, 334-345.
36. Treps, L.; Gomez, A.; de Bruin, T.; Chizallet, C., Environment, Stability and Acidity of External Surface Sites of Silicalite-1 and ZSM-5 Micro and Nano Slabs, Sheets, and Crystals. *ACS Catal.* **2020**, *10*, 3297-3312.
37. Sokol, A. A.; Catlow, C. R. A.; Garcés, J. M.; Kuperman, A., Local States in Microporous Silica and Aluminum Silicate Materials. 1. Modeling Structure, Formation, and Transformation of Common Hydrogen Containing Defects. *J. Phys. Chem. B* **2002**, *106*, 6163-6177.
38. Bučko, T.; Benco, L.; Hafner, J., Defect Sites at the (001) Surface of Mordenite: An Ab Initio Study. *J. Chem. Phys.* **2003**, *118*, 8437-8445.
39. Remy, M.; Genet, M.; Poncelet, G.; Lardinois, P.; Notte, P., Investigation of Dealuminated Mordenites by X-Ray Photoelectron Spectroscopy. *J. Phys. Chem.* **1992**, *96*, 2614-2617.

40. Ravi, M.; Sushkevich, V. L.; van Bokhoven, J. A., Towards a Better Understanding of Lewis Acidic Aluminium in Zeolites. *Nat. Mater.* **2020**, *19*, 1047-1056.
41. Li, S.; Zheng, A.; Su, Y.; Zhang, H.; Chen, L.; Yang, J.; Ye, C.; Deng, F., Brønsted/Lewis Acid Synergy in Dealuminated Hy Zeolite: A Combined Solid-State Nmr and Theoretical Calculation Study. *J. Am. Chem. Soc.* **2007**, *129*, 11161-11171.
42. Yi, X.; Liu, K.; Chen, W.; Li, J.; Xu, S.; Li, C.; Xiao, Y.; Liu, H.; Guo, X.; Liu, S. B., et al., Origin and Structural Characteristics of Tri-Coordinated Extra-Framework Aluminum Species in Dealuminated Zeolites. *J. Am. Chem. Soc.* **2018**, *140*, 10764-10774.
43. Bhering, D. L.; Ramírez-Solís, A.; Mota, C. J. A., A Density Functional Theory Based Approach to Extraframework Aluminum Species in Zeolites. *J. Phys. Chem. B* **2003**, *107*, 4342-4347.
44. Liu, C.; Li, G.; Hensen, E. J. M.; Pidko, E. A., Nature and Catalytic Role of Extraframework Aluminum in Faujasite Zeolite: A Theoretical Perspective. *ACS Catal.* **2015**, *5*, 7024-7033.
45. Du, Y.-J.; Hu, W.-D.; Wang, C.-M.; Zhou, J.; Yang, G.; Wang, Y.-D.; Yang, W.-M., First-Principles Microkinetic Analysis of Lewis Acid Sites in Zn-ZSM-5 for Alkane Dehydrogenation and Its Implication to Methanol-to-Aromatics Conversion. *Catal. Sci. Technol.* **2021**, *11*, 2031-2046.
46. Penzien, J.; Abraham, A.; van Bokhoven, J. A.; Jentys, A.; Müller, T. E.; Sievers, C.; Lercher, J. A., Generation and Characterization of Well-Defined Zn^{2+} Lewis Acid Sites in Ion Exchanged Zeolite Bea. *J. Phys. Chem. B* **2004**, *108*, 4116-4126.
47. Luo, H. Y.; Lewis, J. D.; Roman-Leshkov, Y., Lewis Acid Zeolites for Biomass Conversion: Perspectives and Challenges on Reactivity, Synthesis, and Stability. *Annu Rev Chem Biomol Eng* **2016**, *7*, 663-692.
48. Dapsens, P. Y.; Mondelli, C.; Perez-Ramirez, J., Design of Lewis-Acid Centres in Zeolitic Matrices for the Conversion of Renewables. *Chem. Soc. Rev.* **2015**, *44*, 7025-7043.
49. Muller, S.; Liu, Y.; Kirchberger, F. M.; Tonigold, M.; Sanchez-Sanchez, M.; Lercher, J. A., Hydrogen Transfer Pathways During Zeolite Catalyzed Methanol Conversion to Hydrocarbons. *J. Am. Chem. Soc.* **2016**, *138*, 15994-16003.
50. Liu, Y.; Kirchberger, F. M.; Muller, S.; Eder, M.; Tonigold, M.; Sanchez-Sanchez, M.; Lercher, J. A., Critical Role of Formaldehyde During Methanol Conversion to Hydrocarbons. *Nat. Commun.* **2019**, *10*, 1462.
51. Valecillos, J.; Epelde, E.; Albo, J.; Aguayo, A. T.; Bilbao, J.; Castaño, P., Slowing Down the Deactivation of H-ZSM-5 Zeolite Catalyst in the Methanol-to-Olefin (MTO) Reaction by P or Zn Modifications. *Catal. Today* **2020**, *348*, 243-256.
52. Yarulina, I.; De Wispelaere, K.; Bailleul, S.; Goetze, J.; Radersma, M.; Abou-Hamad, E.; Vollmer, I.; Goesten, M.; Mezari, B.; Hensen, E. J. M., et al., Structure-Performance Descriptors and the Role of Lewis Acidity in the Methanol-to-Propylene Process. *Nat. Chem.* **2018**, *10*, 804-812.
53. Bailleul, S.; Yarulina, I.; Hoffman, A. E. J.; Dokania, A.; Abou-Hamad, E.; Chowdhury, A. D.; Pieters, G.; Hajek, J.; De Wispelaere, K.; Waroquier, M., et al., A Supramolecular View on the Cooperative Role of Bronsted and Lewis Acid Sites in Zeolites for Methanol Conversion. *J. Am. Chem. Soc.* **2019**, *141*, 14823-14842.
54. Chen, X.; Li, R.; Yan, H.; Liu, Y.; Yang, C., A Dft Study for Catalytic Deoxygenation of Methyl Butyrate on a Lewis Acid Site of ZSM-5 Zeolite. *Catalysts* **2020**, *10*.
55. Blaszkowski, S. R.; van Santen, R. A., The Mechanism of Dimethyl Ether Formation from Methanol Catalyzed by Zeolitic Protons. *J. Am. Chem. Soc.* **1996**, *118*, 5152-5153.
56. Masih, D.; Rohani, S.; Kondo, J. N.; Tatsumi, T., Low-Temperature Methanol Dehydration to Dimethyl Ether over Various Small-Pore Zeolites. *Appl. Catal. B* **2017**, *217*, 247-255.
57. Perdew, J. P.; Burke, K.; Ernzerhof, M., Generalized Gradient Approximation Made Simple. *Phys. Rev. Lett.* **1996**, *77 (18)t*, 3865-3868.
58. Grimme, S.; Antony, J.; Ehrlich, S.; Krieg, H., A Consistent and Accurate Ab Initio Parametrization of Density Functional Dispersion Correction (DFT-D) for the 94 Elements H-Pu. *J. Chem. Phys.* **2010**, *132*, 154104.
59. Kresse, G.; Furthmuller, J., Efficient Iterative Schemes for Ab Initio Total-Energy Calculations Using a Plane-Wave Basis Set. *Phys. Rev. B* **1996**, *54*, 11169-11186.
60. Kresse, G.; Joubert, D., From Ultrasoft Pseudopotentials to the Projector Augmented-Wave Method. *Phys. Rev. B* **1999**, *59*, 1758-1775.
61. Hjorth Larsen, A.; Jorgen Mortensen, J.; Blomqvist, J.; Castelli, I. E.; Christensen, R.; Dulak, M.; Friis, J.; Groves, M. N.; Hammer, B.; Hargus, C., et al., The Atomic Simulation Environment-a Python Library for Working with Atoms. *J Phys Condens Matter* **2017**, *29*, 273002.
62. Plessow, P. N., Efficient Transition State Optimization of Periodic Structures through Automated Relaxed Potential Energy Surface Scans. *J. Chem. Theory Comput.* **2018**, *14*, 981-990.
63. Rybicki, M.; Sauer, J., Ab Initio Prediction of Proton Exchange Barriers for Alkanes at Bronsted Sites of Zeolite H-MFI. *J. Am. Chem. Soc.* **2018**, *140*, 18151-18161.
64. Goncalves, T. J.; Plessow, P. N.; Studt, F., On the Accuracy of Density Functional Theory in Zeolite Catalysis. *Chemcatchem* **2019**, *11*, 4368-4376.
65. Neese, F., The Orca Program System. *Wiley Interdiscip. Rev. Comput. Mol. Sci.* **2012**, *2*, 73-78.
66. Dunning, T. H., Gaussian Basis Sets for Use in Correlated Molecular Calculations. I. The Atoms Boron through Neon and Hydrogen. *J. Chem. Phys.* **1989**, *90*, 1007.
67. Minenkov, Y.; Bistoni, G.; Riplinger, C.; Auer, A. A.; Neese, F.; Cavallo, L., Pair Natural Orbital and Canonical Coupled Cluster Reaction Enthalpies Involving Light to Heavy Alkali and Alkaline Earth Metals: The Importance of Sub-Valence Correlation. *Phys. Chem. Chem. Phys.* **2017**, *19*, 9374-9391.
68. Riplinger, C.; Pinski, P.; Becker, U.; Valeev, E. F.; Neese, F., Sparse Maps--A Systematic Infrastructure for Reduced-Scaling Electronic Structure Methods. II. Linear Scaling Domain Based Pair Natural Orbital Coupled Cluster Theory. *J. Chem. Phys.* **2016**, *144*, 024109.
69. Saitow, M.; Becker, U.; Riplinger, C.; Valeev, E. F.; Neese, F., A New near-Linear Scaling, Efficient and Accurate, Open-Shell Domain-Based Local Pair Natural Orbital Coupled Cluster Singles and Doubles Theory. *J. Chem. Phys.* **2017**, *146*, 164105.
70. Neese, F.; Wennmohs, F.; Hansen, A.; Becker, U., Efficient, Approximate and Parallel Hartree–Fock and Hybrid DFT Calculations. A 'Chain-of-Spheres' Algorithm for the Hartree–Fock Exchange. *Chem. Phys.* **2009**, *356*, 98-109.
71. Weigend, F.; Furche, F.; Ahlrichs, R., Gaussian Basis Sets of Quadruple Zeta Valence Quality for Atoms H–Kr. *J. Chem. Phys.* **2003**, *119*, 12753.
72. Weigend, F.; Ahlrichs, R., Balanced Basis Sets of Split Valence, Triple Zeta Valence and Quadruple Zeta Valence Quality for H to Rn: Design and Assessment of Accuracy. *Phys. Chem. Chem. Phys.* **2005**, *7*, 3297-3305.
73. Eichkorn, K.; Treutler, O.; Öhm, H.; Häser, M.; Ahlrichs, R., Auxiliary Basis Sets to Approximate Coulomb Potentials. *Chem. Phys. Lett.* **1995**, *240*, 283-290.
74. *Turbomole*, V7.4.1; TURBOMOLE GmbH: 2019.
75. Keil, F. J., Methanol-to-Hydrocarbons: Process Technology. *Microporous Mesoporous Mater.* **1999**, *29*, 49-66.
76. Jones, A. J.; Iglesia, E., Kinetic, Spectroscopic, and Theoretical Assessment of Associative and Dissociative Methanol Dehydration Routes in Zeolites. *Angew. Chem. Int. Ed. Engl.* **2014**, *53*, 12177-12181.
77. Rey, J.; Raybaud, P.; Chizallet, C., Ab Initio Simulation of the Acid Sites at the External Surface of Zeolite Beta. *ChemCatChem* **2017**, *9*, 2176-2185.
78. Chizallet, C., Toward the Atomic Scale Simulation of Intricate Acidic Aluminosilicate Catalysts. *ACS Catal.* **2020**, *10*, 5579-5601.
79. Treps, L.; Demaret, C.; Wisser, D.; Harbuzaru, B.; Méthivier, A.; Guillon, E.; Benedis, D. V.; Gomez, A.; Bruin, T. d.; Rivallan, M., et al., Spectroscopic Expression of the External Surface Sites of H-ZSM-5. *J. Phys. Chem. C* **2021**, *125*, 2163-2181.
80. Sommer, L.; Mores, D.; Svelle, S.; Stöcker, M.; Weckhuysen, B. M.; Olsbye, U., Mesopore Formation in Zeolite H-

SSZ-13 by Desilication with Naoh. *Microporous Mesoporous Mater.* **2010**, *132*, 384-394.
81. Zhang, L.; Wang, H., In Situ Synthesis of Alpo4-14, Coapo-44 and Znapo-34 Films on Alumina Substrates. *J. Mater. Sci* **2002**, *37*, 1491-1496.
82. Guo, X.; Xu, M.; She, M.; Zhu, Y.; Shi, T.; Chen, Z.; Peng, L.; Guo, X.; Lin, M.; Ding, W., Morphology-Reserved Synthesis of Discrete Nanosheets of CuO@SAPO-34 and Pore Mouth Catalysis for One-Pot Oxidation of Cyclohexane. *Angew. Chem. Int. Ed. Engl.* **2020**, *59*, 2606-2611.
83. Ghobarkar, H.; Schäf, O.; Knauth, P., Zeolite Synthesis by the High-Pressure Hydrothermal Method: Synthesis of Natural 6-Ring Zeolites with Different Void Systems. *Angew. Chem. Int. Ed.* **2001**, *40*.
84. Nguyen, H. G.; Konya, G.; Eyring, E. M.; Hunter, D. B.; Truong, T. N., Theoretical Study on the Interaction between Xenon and Positively Charged Silver Clusters in Gas Phase and on the (001) Chabazite Surface. *J. Phys. Chem. C* **2009**, *113*.
85. Castellà-Ventura, M.; Akacem, Y.; Kassab, E., Vibrational Analysis of Pyridine Adsorption on the Brønsted Acid Sites of Zeolites Based on Density Functional Cluster Calculations. *J. Phys. Chem. C* **2008**, *112*, 19045–19054.
86. Lercher, J. A.; Gründling, C.; Eder-Mirth, G., Infrared Studies of the Surface Acidity of Oxides and Zeolites Using Adsorbed Probe Molecules. *Catal. Today* **1996**, *27*, 353-376.
87. Wu, W.; Weitz, E., Modification of Acid Sites in Zsm-5 by Ion-Exchange: An in-Situ Ftir Study. *Appl. Surf. Sci.* **2014**, *316*, 405-415.
88. El-Malki, E.-M.; van Santen, R. A.; Sachtler, W. M. H., Introduction of Zn, Ga, and Fe into HZSM-5 Cavities by Sublimation: Identification of Acid Sites. *J. Phys. Chem. B* **1999**, *103*, 4611-4622.
89. Kline, C. H.; Turkevich, J., The Vibrational Spectrum of Pyridine and the Thermodynamic Properties of Pyridine Vapors. *J. Chem. Phys.* **1944**, *12*, 300.
90. Stoyanov, S. R.; Gusarov, S.; Kuznicki, S. M.; Kovalenko, A., Theoretical Modeling of Zeolite Nanoparticle Surface Acidity for Heavy Oil Upgrading. *J. Phys. Chem. C* **2008**, *112*, 6794-6810.
91. Carr, R. T.; Neurock, M.; Iglesia, E., Catalytic Consequences of Acid Strength in the Conversion of Methanol to Dimethyl Ether. *J. Catal.* **2011**, *278*, 78-93.
92. Migliori, M.; Aloise, A.; Catizzone, E.; Giordano, G., Kinetic Analysis of Methanol to Dimethyl Ether Reaction over H-MFI Catalyst. *Ind. Eng. Chem. Res.* **2014**, *53*, 14885-14891.
93. Moses, P. G.; Nørskov, J. K., Methanol to Dimethyl Ether over ZSM-22: A Periodic Density Functional Theory Study. *ACS Catal.* **2013**, *3*, 735-745.
94. Sandre, E.; Payne, M. C.; Gale, J. D., First Principles Location of the Transition State for Formation of Dimethyl Ether in a Zeolite. *Chem. Commun.* **1998**, 2445-2446.
95. Di Iorio, J. R.; Hoffman, A. J.; Nimlos, C. T.; Nystrom, S.; Hibbitts, D.; Gounder, R., Mechanistic Origins of the High-Pressure Inhibition of Methanol Dehydration Rates in Small-Pore Acidic Zeolites. *J. Catal.* **2019**, *380*, 161-177.
96. DeLuca, M.; Kravchenko, P.; Hoffman, A.; Hibbitts, D., Mechanism and Kinetics of Methylating C6–C12 Methylbenzenes with Methanol and Dimethyl Ether in H-MFI Zeolites. *ACS Catal.* **2019**, *9*, 6444-6460.
97. Fečík, M.; Plessow, P. N.; Studt, F., A Systematic Study of Methylation from Benzene to Hexamethylbenzene in H-SSZ-13 Using Density Functional Theory and Ab Initio Calculations. *ACS Catal.* **2020**, *10*, 8916-8925.
98. Mazar, M. N.; Al-Hashimi, S.; Bhan, A.; Cococcioni, M., Methylation of Ethene by Surface Methoxides: A Periodic PBE+D Study across Zeolites. *J. Phys. Chem. C* **2012**, *116*, 19385-19395.
99. Bobuatong, K.; Probst, M.; Limtrakul, J., Structures and Energetics of the Methylation of 2-Methylnaphthalene with Methanol over H-Bea Zeolite. *J. Phys. Chem. C* **2010**, *114*, 21611–21617.
100. Ahn, J. H.; Kolvenbach, R.; Gutiérrez, O. Y.; Al-Khattaf, S. S.; Jentys, A.; Lercher, J. A., Tailoring P-Xylene Selectivity in Toluene Methylation on Medium Pore-Size Zeolites. *Microporous Mesoporous Mater.* **2015**, *210*, 52-59.
101. Svelle, S.; Arstad, B.; Kolboe, S.; Swang, O., A Theoretical Investigation of the Methylation of Alkenes with Methanol over Acidic Zeolite. *J. Phys. Chem. B* **2003**, *107*, 9281-9289.
102. Svelle, S.; Tuma, C.; Rozanska, X.; Kerber, T.; Sauer, J., Quantum Chemical Modeling of Zeolite-Catalyzed Methylation Reactions: Toward Chemical Accuracy for Barriers. *J. Am. Chem. Soc.* **2009**, *131*, 816–825.
103. Zhao, Z.; Shi, H.; Wan, C.; Hu, M. Y.; Liu, Y.; Mei, D.; Camaioni, D. M.; Hu, J. Z.; Lercher, J. A., Mechanism of Phenol Alkylation in Zeolite H-Bea Using in Situ Solid-State Nmr Spectroscopy. *J. Am. Chem. Soc.* **2017**, *139*, 9178-9185.
104. Arvidsson, A. A.; Plessow, P. N.; Studt, F.; Hellman, A., Influence of Acidity on the Methanol-to-DME Reaction in Zeotypes: A First Principles-Based Microkinetic Study. *J. Phys. Chem. C* **2020**, *124*, 14658-14663.
105. Fečík, M.; Plessow, P. N.; Studt, F., Simple Scheme to Predict Transition-State Energies of Dehydration Reactions in Zeolites with Relevance to Biomass Conversion. *J. Phys. Chem. C* **2018**, *122*, 23062-23067.
106. Kozuch, S.; Shaik, S., How to Conceptualize Catalytic Cycles? The Energetic Span Model. *Acc. Chem. Res.* **2010**, *44*, 101-110.
107. Wang, W.; Buchholz, A.; Seiler, M.; Hunger, M., Evidence for an Initiation of the Methanol-to-Olefin Process by Reactive Surface Methoxy Groups on Acidic Zeolite Catalysts. *J. Am. Chem. Soc.* **2003**, *125*, 15260-15267.
108. Wang, W.; Jiang, Y.; Hunger, M., Mechanistic Investigations of the Methanol-to-Olefin (MTO) Process on Acidic Zeolite Catalysts by in Situ Solid-State Nmr Spectroscopy. *Catal. Today* **2006**, *113*, 102-114.
109. Martínez-Espín, J. S.; De Wispelaere, K.; Janssens, T. V. W.; Svelle, S.; Lillerud, K. P.; Beato, P.; Van Speybroeck, V.; Olsbye, U., Hydrogen Transfer Versus Methylation: On the Genesis of Aromatics Formation in the Methanol-to-Hydrocarbons Reaction over H-ZSM-5. *ACS Catal.* **2017**, *7*, 5773-5780.
110. Plessow, P. N.; Studt, F., Olefin Methylation and Cracking Reactions in H-SSZ-13 Investigated with Ab Initio and DFT Calculations. *Catal. Sci. Technol.* **2018**, *8*, 4420-4429.

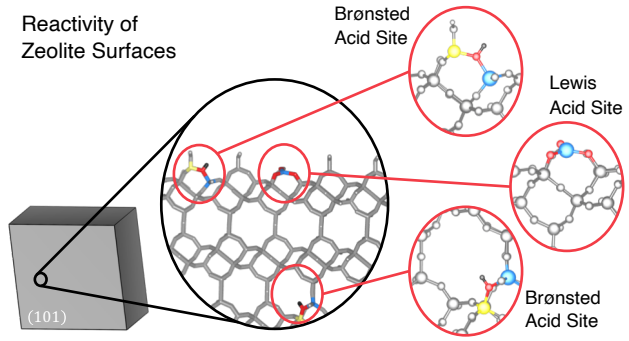
Reactivity of
Zeolite Surfaces
Brønsted
Acid Site
Lewis
Acid Site
Brønsted
Acid Site
(101)

TOC Graphic